

Article

Design of a MIMO Antenna with High Gain and Enhanced Isolation for WLAN Applications

He Peng, Ruixing Zhi, Qichao Yang, Jing Cai, Yi Wan and Gui Liu *

College of Electrical and Electronics Engineering, Wenzhou University, Wenzhou 325035, China; 184511087167@stu.wzu.edu.cn (H.P.); 16451186183@stu.wzu.edu.cn (R.Z.); 194511881381@stu.wzu.edu.cn (Q.Y.); 20451941040@stu.wzu.edu.cn (J.C.); jsj_yiwan@wzu.edu.cn (Y.W.)

* Correspondence: gliu@wzu.edu.cn

Abstract: A multi-input multi-output (MIMO) antenna for wireless local area network (WLAN) applications operating in 2.4 GHz and 5.8 GHz frequency bands is proposed in this paper. The proposed dual-band MIMO antenna is composed of two symmetrical radiation elements, and the isolation performance is improved by adopting parasitic elements and a defective ground plane. The measured reflection coefficients are less than -10 dB in the bandwidth range of 2.12–2.8 GHz and 4.95–6.65 GHz, respectively. The measurements show excellent isolation of -21 dB and -15 dB in both desired frequency bands, respectively. The total peak gain is greater than 4.8 dBi. The calculated envelope correlation coefficients (ECC), based on the measured S-parameters, are smaller than 0.01 and 0.024 in the lower and higher frequency bands, respectively. The dimension of the presented antenna occupies $50 \times 40 \times 1.59$ mm³. It is suitable for IEEE 802.11 a/b/g/n (2.4–2.4835 GHz, 5.15–5.35 GHz and 5.725–5.85 GHz) WLAN applications.

Keywords: multiple-input multiple-output (MIMO); wireless local area network (WLAN); dual-band antenna; IEEE 802.11



check for updates

Citation: Peng, H.; Zhi, R.; Yang, Q.; Cai, J.; Wan, Y.; Liu, G. Design of a MIMO Antenna with High Gain and Enhanced Isolation for WLAN Applications. *Electronics* **2021**, *10*, 1659. <https://doi.org/10.3390/electronics10141659>

Academic Editor: Emilio Arneri

Received: 7 May 2021

Accepted: 8 July 2021

Published: 12 July 2021

Publisher's Note: MDPI stays neutral with regard to jurisdictional claims in published maps and institutional affiliations.



Copyright: © 2021 by the authors. Licensee MDPI, Basel, Switzerland. This article is an open access article distributed under the terms and conditions of the Creative Commons Attribution (CC BY) license (<https://creativecommons.org/licenses/by/4.0/>).

1. Introduction

In recent years, the available wireless communication spectrum has faced a high degree of traffic limitation due to rapid growth in the number of subscribers, and the need for a higher data transmission rate, better reliability and spectrum allocation efficiency has stimulated considerable research on multiple-input multiple-output technology [1–3]. In addition, in order to enable modern mobile devices to operate at multiple frequencies, miniaturized multi-band antennas are required.

It is challenging work to improve the isolation of a MIMO antenna, and so various methods have been proposed [1–11]. Several decoupling technologies, such as a neutralization line (NL) [2,3], parasitic elements [4,5] and a defected ground structure (DGS) [6–8], have been presented. However, decoupling technology requires a certain amount of space to increase isolation, which limits the miniaturization of the antenna. In addition, some shapes of isolation elements have also been used to improve MIMO performance, such as quasi-loops on the outermost ground planes [9], a T-shaped slot on the ground plane [10] and four identical octagonal-shaped radiating elements [11]. Recently, metamaterials [12] have been applied to various mobile terminals, such as artificial magnetic conductor (AMC) [13], also called meta-surface or reactive impedance surface (RIS) [14]. Nevertheless, a method of designing antennas with miniaturized, excellent isolation and low correlation is still a challenge [15,16].

In this work, a dual-band high-gain MIMO antenna, which occupies an area of 50×40 mm, is presented. The antenna element is composed of two semicircular annulars with rectangular microstrips. The two elements of the antenna are placed symmetrically, and a pair of h-shaped slots are etched on the ground plane. The defects on the ground affect the current distribution, reduce the coupling between ports and increase the isolation

to improve the antenna radiation efficiency. The polarization of the proposed antenna is linear polarization. It shows excellent antenna performance at 2.4 GHz and 5.8 GHz, especially in terms of gain better than 4.8 dBi and isolation better than 15 dB, respectively.

2. Antenna Design

Table 1 shows some performance requirements of the MIMO antenna design process. The simulation software of this antenna design is high-frequency structure simulation (HFSS).

Table 1. Some performance requirements of the antenna.

Types of Antenna	WLAN MIMO Antenna
Frequency	2.4–2.4385 GHz and 5.725–5.8 GHz
Isolation (dB)	>15 dB
ECC	<0.3

Figure 1 shows the geometry of the proposed dual-band MIMO antenna. The antenna was fabricated on a FR4 substrate with ϵ_r of 4.4, $\tan \delta$ of 0.02 and a thickness of 1.59 mm. The proposed antenna radiation element consists of a pair of symmetrical semicircular annular microstrip lines and zigzag rectangular microstrip lines, which cleverly allocates higher and lower frequencies to different locations on the top view of the substrate. The feed lines with a width of 3 mm are used for better impedance matching. On the bottom view of the substrate, the methods of isolation are to etch two symmetrical h-shaped slots on the ground plane and to form a fork-shaped microstrip line.

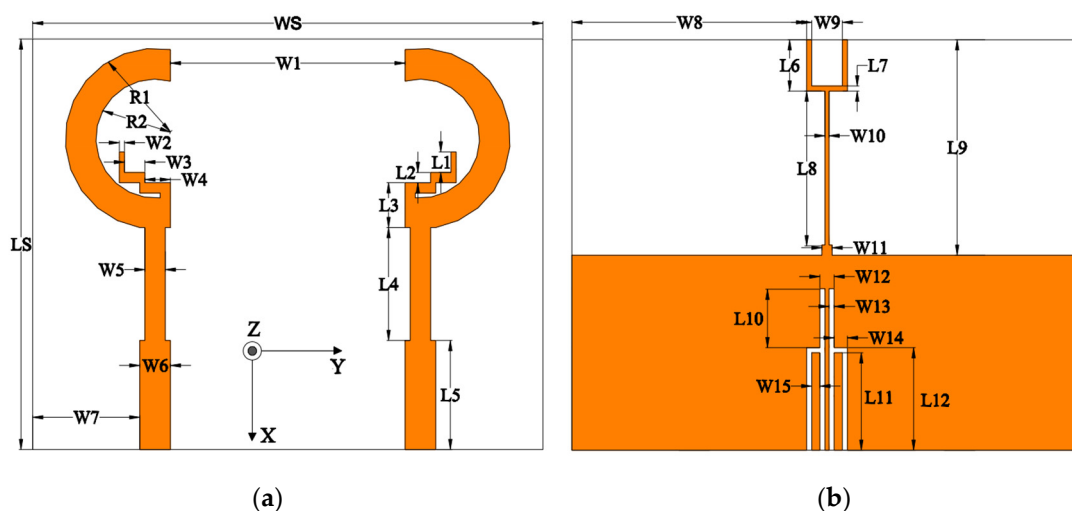
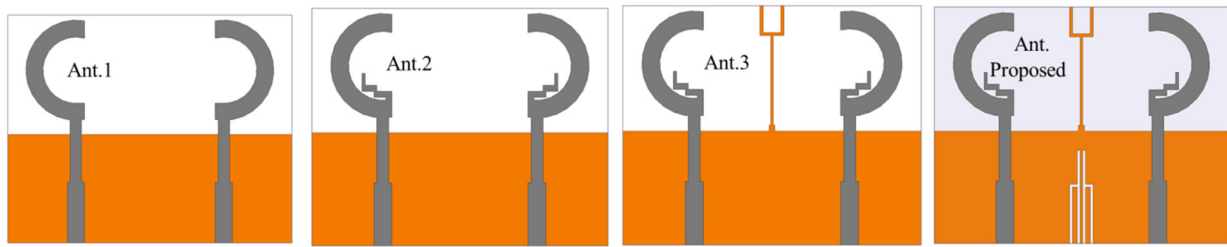
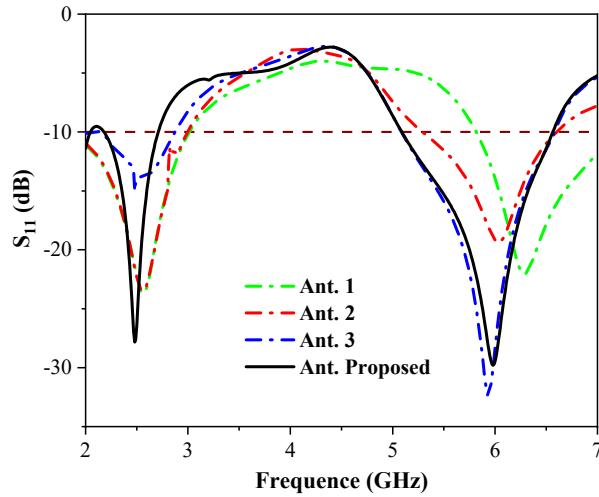


Figure 1. Geometry of the proposed antenna. (a) Top view; (b) bottom view.

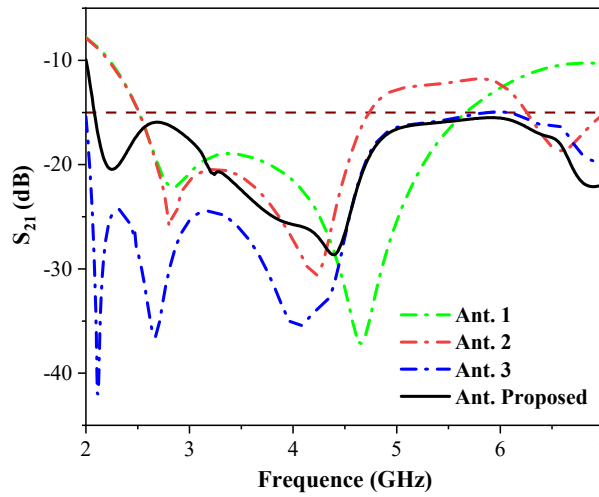
As shown in Figure 2, the evolution of the designed antenna structure and simulated S_{11} and S_{22} are listed. The introduction of the zigzag rectangular microstrip lines in Ant. 2 can tune both the S_{11} and the S_{22} of Ant. 1 to the higher frequencies in the higher frequency band, while those in the lower frequency band remain almost unchanged. The introduction of the fork-shaped microstrip line in Ant. 3 can be used to improve the isolation S_{21} of the Ant. 2. However, the S_{11} of Ant. 3 in the lower-frequency band deteriorates to a certain extent. Finally, the two symmetrical h-shaped slots on the ground plane reduce the influence of the neutralization current on the S_{11} , so that the S_{11} parameter in the lower-frequency band is significantly improved.



(a)



(b)



(c)

Figure 2. Evolution of the proposed antenna. (a) Structure of antenna 1, 2 and 3 and proposed; (b) simulated S_{11} ; (c) simulated S_{21} .

In a radiation unit, the value of width, $W5$, can be used to adjust the bandwidth of the resonant frequencies. Figure 3a shows the simulated reflection coefficients of the proposed antenna with different values of $W5$. It can be seen that the -10 dB bandwidth fully meets the required frequency band at 2.4–2.4835 GHz when the $W5$ is 2 mm. Figure 3b shows the isolation S_{21} is less than -15 dB at all required bands.

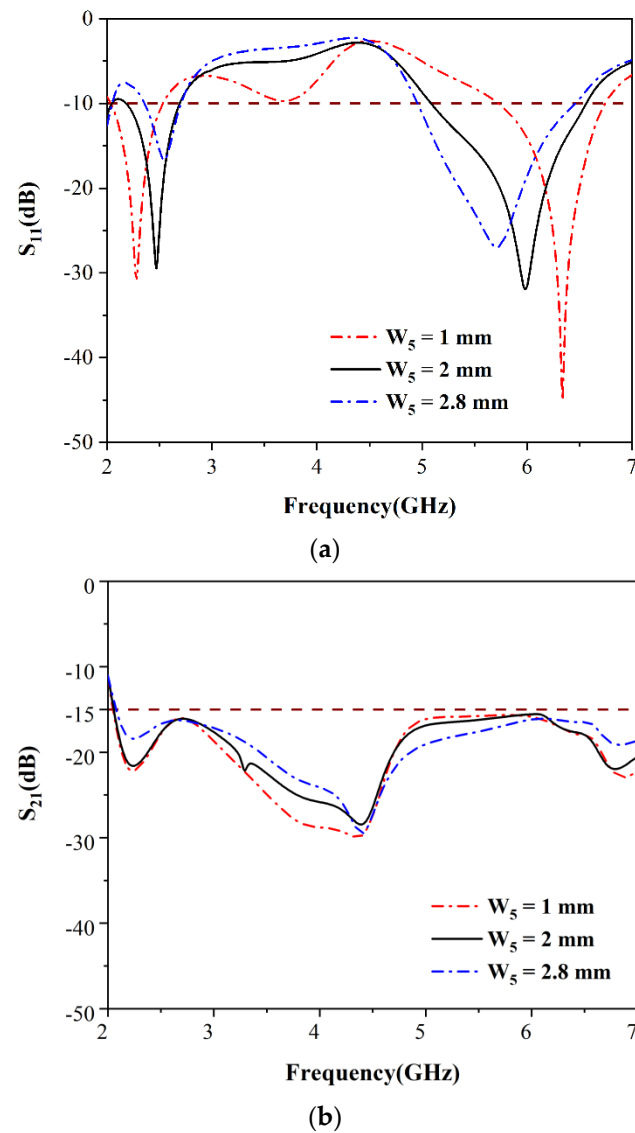


Figure 3. Simulated parameters with different values of W_5 . (a) Reflection coefficients; (b) isolation.

Adjusting the frequency of the higher-frequency band, as shown in Figure 4a, can be achieved by optimizing the value of R_1 , while the lower frequency band is unchanged. After optimization, the optimal size of the parameter R is 8.8 mm. The -10 dB impedance bandwidth can meet the requirements of band coverage. Figure 4b shows the isolation S_{21} is less than -15 dB at all required bands as well.

Figure 5 shows the simulated current distribution of the antenna. When the antenna functions at 2.4 GHz, the current is mainly concentrated on the entire semicircular annular. When the frequency rises to 5.5 GHz, the current is concentrated on the rectangular rod.

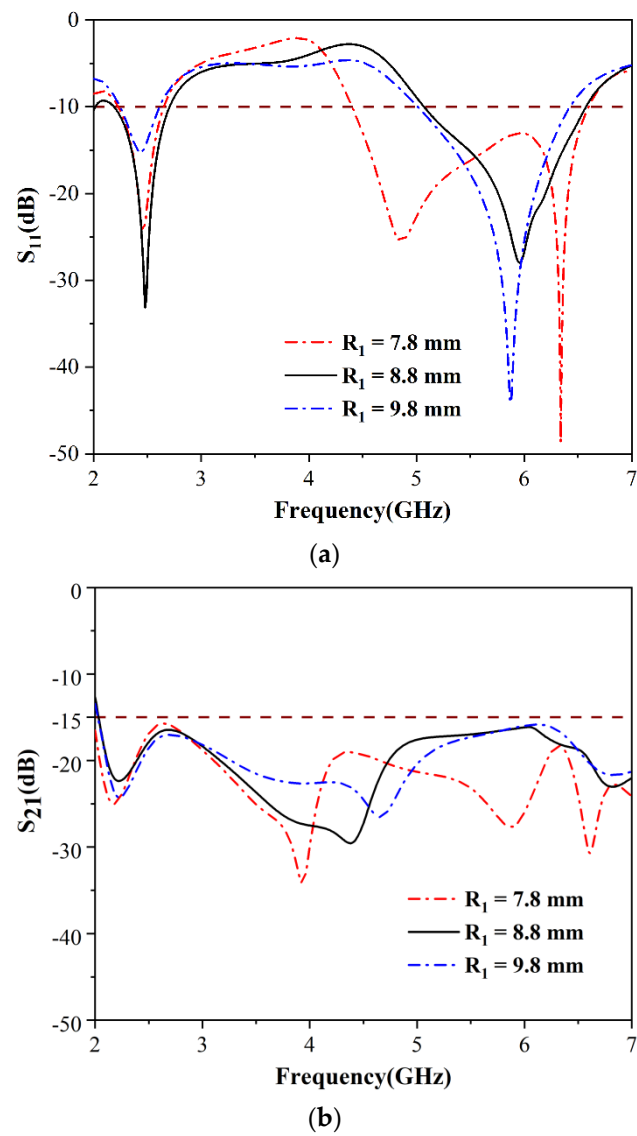


Figure 4. Simulated parameters with different values of R_1 . (a) Reflection coefficients; (b) isolation.

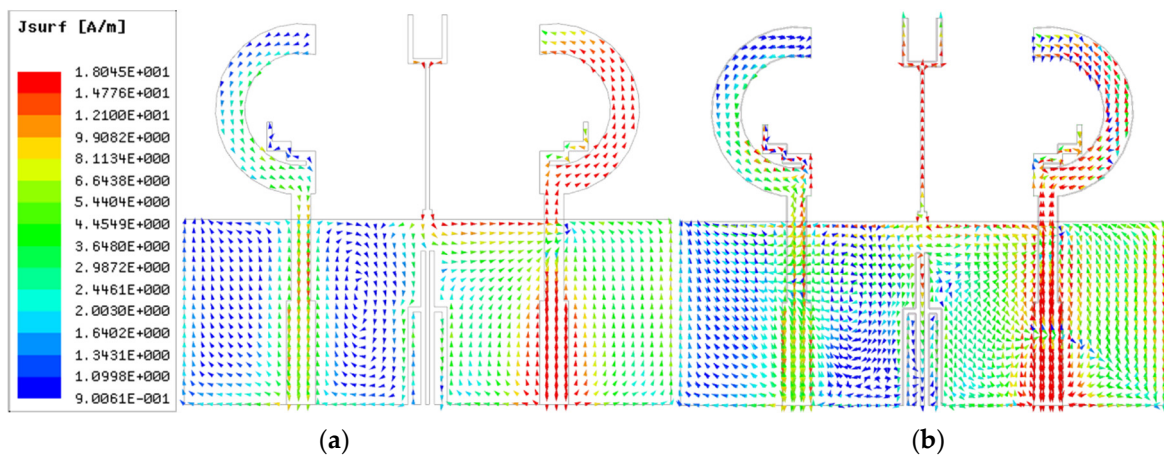


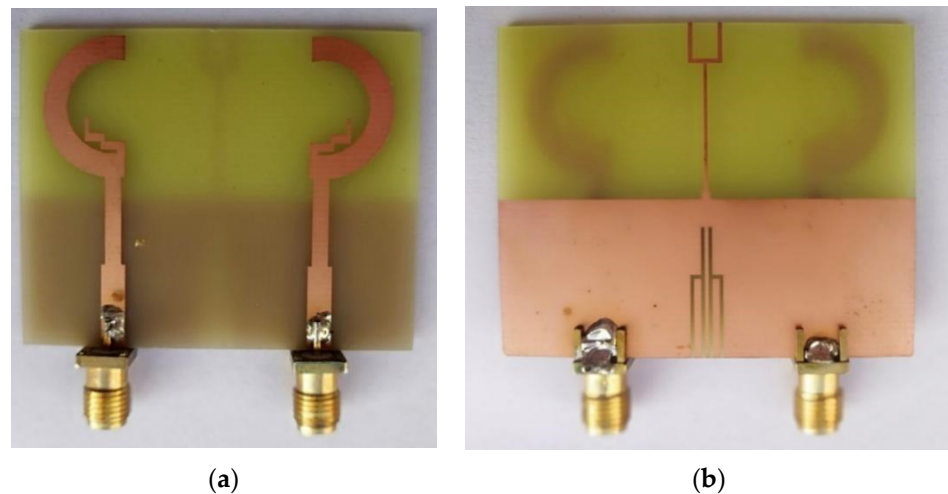
Figure 5. Simulated current distribution at two frequencies. (a) 2.4 GHz; (b) 5.5 GHz.

The optimized antenna dimensions (in millimeters) are shown in Table 2.

Table 2. Parameters of the proposed antenna (unit: mm).

Parameters	Value	Parameters	Value	Parameters	Value
W_1	23	W_2	0.5	W_3	2
W_4	2.5	W_5	2	W_6	3
W_7	10.5	W_8	23	W_9	3
W_{10}	0.4	W_{11}	9.5	W_{12}	1.4
W_{13}	0.5	W_{14}	1.3	W_{15}	0.8
L_1	2	L_2	1	L_3	4.4
L_4	11	L_5	10.6	L_6	5
L_7	0.5	L_8	15	L_9	21
L_{10}	5.7	L_{11}	9.5	L_{12}	
R_1	8.8	R_2	5.8		

Figure 6 shows the actual shape of the proposed antenna.

**Figure 6.** The actual picture of the antenna. (a) Top view; (b) bottom view.

3. Results and Discussion

The S-parameters of the antenna port are measured by the PNA N5224A network analyzer. The measurement results are compared with the simulation results. Figure 7 shows the simulated and measured reflection coefficients S_{11} of the proposed antenna. The measured -10 dB impedance bandwidths are 680 MHz (2.12–2.8 GHz) and 1700 MHz (4.95–6.65 GHz) in the desired frequency bands, respectively. When the reflection coefficient of the port is tested, the measured results have a shift of the resonant frequencies compared with the simulation. The S_{11} is less than -10 dB, which meets the requirements in both bands of interest.

As shown in Figure 8, the isolation of the antenna can be evaluated by S_{21} . The measured S_{21} at the operating frequency bands (2.4–2.4835 GHz and 5.15–5.85 GHz) are less than -15 dB.

Figure 9 shows the measurement results of the peak gain and efficiency of the proposed antenna. It can be seen that the peak gain and radiation efficiency have the same trend. The measured peak gains are about 6.4 dBi and 4.8 dBi in the frequency band required, and the radiation efficiencies at this time are 68.26% (65.03~75%) and 51.36% (48.60~52.28%), respectively.

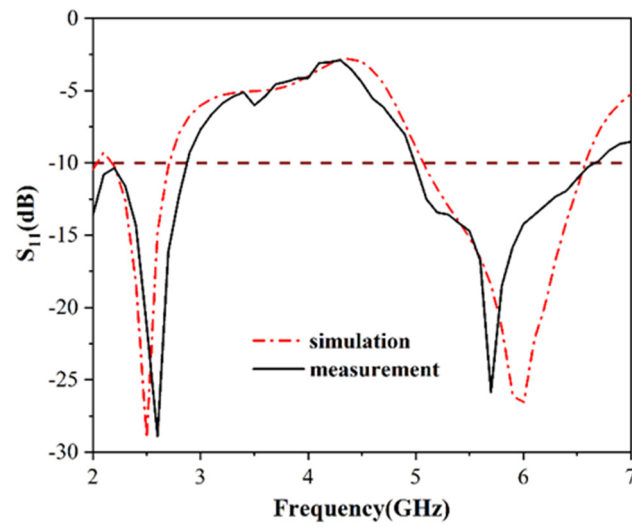


Figure 7. Simulated and measured reflection coefficients of the proposed antenna.

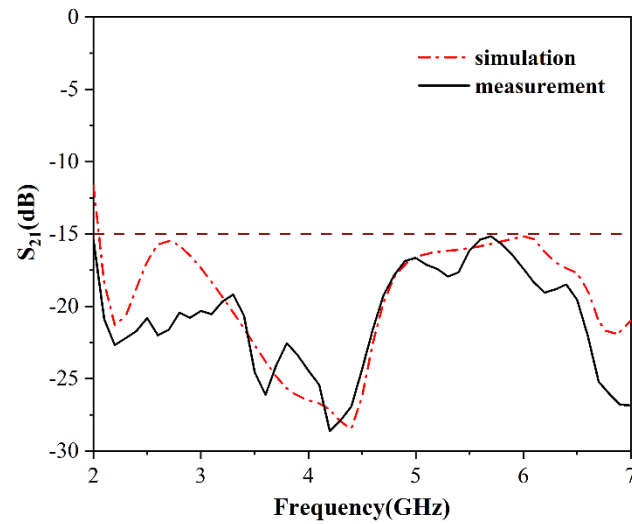


Figure 8. Simulated and measured isolation of the proposed antenna.

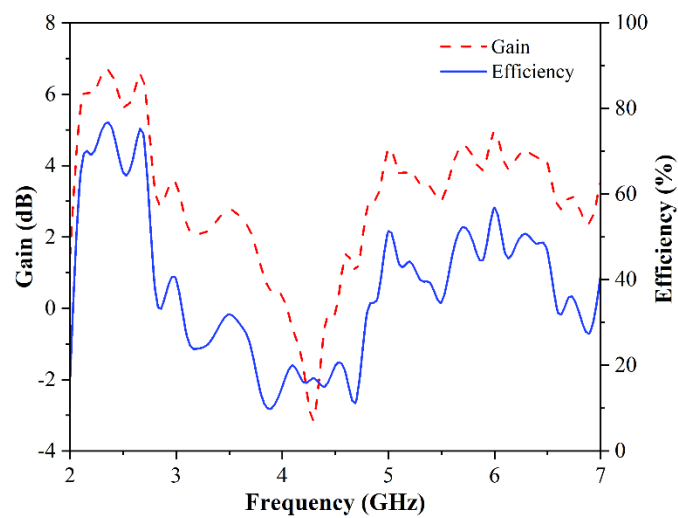


Figure 9. Measured peak gain and radiation efficiency.

The proposed antenna test environment is carried out in a microwave anechoic chamber. Since the two antenna elements have the same structure and size, one port is excited, and the other port is connected by a 50 Ω load terminal. Figure 10 shows the normalized radiation polarization of the antenna operating at 2.4 GHz and 5.5 GHz. Co-polarization and cross-polarization are demonstrated by a black solid line and a red dashed line, respectively. It can be observed that the antenna presents a half-end fire radiation pattern on the E plane and a quasi-omnidirectional radiation pattern on the h plane. The welding effect of the SMA connector may cause the deterioration of the high-frequency radiation pattern.

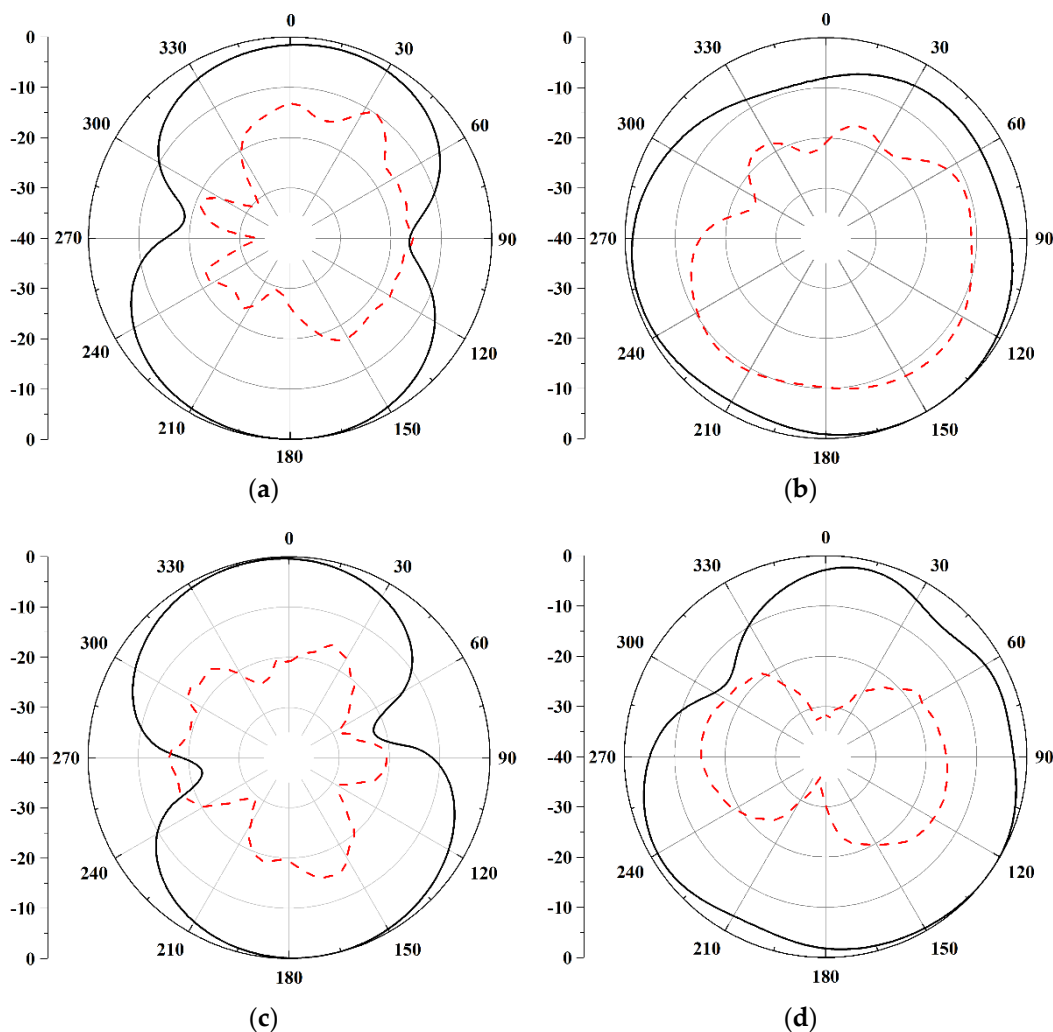


Figure 10. Radiation polarization of the proposed antenna. (a) 2.4 GHz E-plane; (b) 2.4 GHz H-plane; (c) 5.5 GHz E-plane; (d) 5.5 GHz H-plane.

The envelope correlation coefficient (ECC) is a significant parameter used to describe the degree of correlation between communication channels. Taking the proposed dual-element MIMO antenna as an example, its ECC value can be expressed as:

$$\rho_e = \frac{|S_{11}^* S'_{12} + S_{21}^* S'_{22}|^2}{(1 - (|S_{11}|^2 + |S_{21}|^2))(1 - (|S_{22}|^2 + |S_{12}|^2))} \tag{1}$$

where S_{11}^* and S_{21}^* are the imaginary parts of S_{11} and S_{21} parameters, respectively. S'_{12} and S'_{22} are the real parts of S_{12} and S_{22} parameters, respectively.

In general, an ECC value of less than 0.3 is within the limits [17,18]. For a wireless communication system, the lower envelope coefficient can obtain the larger channel capacity. Figure 11 shows the calculated ECC values of the fabricated antenna, which are smaller than 0.01 and 0.024 at 2.4 GHz and 5.5 GHz, respectively.

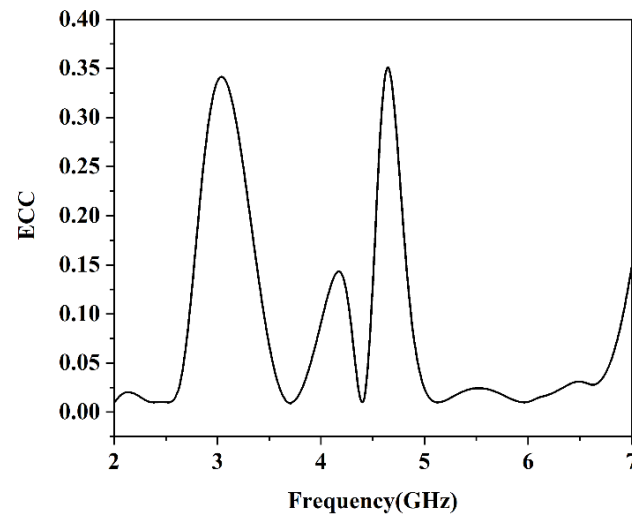


Figure 11. Calculated ECC of the MIMO antenna system.

In Table 3, the operating frequency band, minimum isolation, peak gain and size of the proposed antenna are compared with some recently reported dual-band MIMO antennas. The results show that the proposed design exhibits good performance in peak gain.

Table 3. Performance comparison with recently published work.

Reference	Operating Frequency Bands (GHz)	Minimum Isolation (dB)	Peak Gain (dBi)	Size (mm ³)
[4]	2.2–3.8 5.7–6.2	>15	2.8	30 × 26 × 1.6
[6]	1.73–2.28 2.45	>10	2.33	50 × 110 × 1.56
[10]	2.9–5.3 5.3–5.8	>14	4	26 × 26 × 0.762
[16]	2.25–3.15 4.89–5.95	>15	5.59 5.63	50 × 50 × 1.59
This work	2.12–2.8 4.95–6.65	>15	6.4	50 × 40 × 1.59

4. Conclusions

A novel dual-band MIMO antenna is presented in this paper. The antenna uses a pair of symmetrical antenna elements to radiate the frequency band of interest, and the parasitic elements and defective ground form an outstanding isolation of better than 15 dB, which improves the radiation efficiency of the proposed antenna. The measured –10 dB impedance bandwidth can cover the 2.4 GHz and 5.5 GHz WLAN frequency band. The ECC, calculated based on measured S-parameters, is within the acceptable threshold. The comparison between measurement results and simulation results is relatively successful. The proposed antenna has excellent characteristics for WLAN applications.

Author Contributions: Conceptualization, H.P. and R.Z.; methodology, H.P.; data curation, R.Z. and Q.Y.; investigation, J.C.; measurement, J.C.; writing—original draft preparation, H.P.; writing—review

and editing, Y.W.; supervision and funding acquisition, G.L. All authors have read and agreed to the published version of the manuscript.

Funding: This research work was partially funded by the Science and Technology Department of Zhejiang Province under Grant No. LGG19F010009, National Natural Science Foundation of China under Grant No. 61671330, and Wenzhou Municipal Science and Technology Program under Grant No. C20170005 and No.2018ZG019.

Data Availability Statement: The data supporting this research article are available upon request to the corresponding author.

Conflicts of Interest: The authors declare that there is no conflict of interests regarding the publication of this manuscript.

References

1. Huang, J.; Dong, G.; Cai, J.; Li, H.; Liu, G. A Quad-Port Dual-Band MIMO Antenna Array for 5G Smartphone Applications. *Electronics* **2021**, *10*, 542. [[CrossRef](#)]
2. Li, M.; Jiang, L.; Yeung, K.L. A General and Systematic Method to Design Neutralization Lines for Isolation Enhancement in MIMO Antenna Arrays. *IEEE Trans. Veh. Technol.* **2020**, *69*, 6242–6253. [[CrossRef](#)]
3. Yang, R.; Xi, S.; Cai, Q.; Chen, Z.; Wang, X.; Liu, G. A Compact Planar Dual-Band Multiple-Input and Multiple-Output Antenna with High Isolation for 5G and 4G Applications. *Micromachines* **2021**, *12*, 544. [[CrossRef](#)] [[PubMed](#)]
4. Nirmal, P.C.; Nandgaonkar, A.B.; Nalbalwar, S.; Gupta, R.K. A Compact Dual Band and MIMO Antenna with Improved Isolation for WI-MAX and WLAN Applications. *Prog. Electromagn. Res. M* **2018**, *68*, 69–77. [[CrossRef](#)]
5. Tran, H.H.; Nguyen-Trong, N. Performance Enhancement of MIMO Patch Antenna Using Parasitic Elements. *IEEE Access* **2021**, *9*, 30011–30016. [[CrossRef](#)]
6. Hussain, R.; Khan, M.U.; Sharawi, M.S. An Integrated Dual MIMO Antenna System with Dual-Function GND-Plane Frequency-Agile Antenna. *IEEE Antennas Wirel. Propag. Lett.* **2018**, *17*, 142–145. [[CrossRef](#)]
7. Gao, D.; Cao, Z.X.; Fu, S.D.; Quan, X.; Chen, P. A Novel Slot-Array Defected Ground Structure for Decoupling Microstrip Antenna Array. *IEEE Trans. Antennas Propag.* **2020**, *68*, 7027–7038. [[CrossRef](#)]
8. Zeng, J.; Luk, K. A Simple Wideband Magnetolectric Dipole Antenna with a Defected Ground Structure. *IEEE Antennas Wirel. Propag. Lett.* **2018**, *17*, 1497–1500. [[CrossRef](#)]
9. Ullah, U.; Al-Hasan, M.; Koziel, S.; Mabrouk, I.B. Circular Polarization Diversity Implementation for Correlation Reduction in Wideband Low-Cost Multiple-Input-Multiple-Output Antenna. *IEEE Access* **2020**, *8*, 95585–95593. [[CrossRef](#)]
10. Li, Z.; Yin, C.; Zhu, X. Compact UWB MIMO Vivaldi Antenna with Dual Band-Notched Characteristics. *IEEE Access* **2019**, *7*, 38696–38701. [[CrossRef](#)]
11. Kumar, P.; Urooj, S.; Alrowais, F. Design and Implementation of Quad-Port MIMO Antenna with Dual-Band Elimination Characteristics for Ultra-Wideband Applications. *Appl. Sci.* **2020**, *10*, 1715. [[CrossRef](#)]
12. Iqbal, A.; A Saraereh, O.; Bouazizi, A.; Basir, A. Metamaterial-Based Highly Isolated MIMO Antenna for Portable Wireless Applications. *Electronics* **2018**, *7*, 267. [[CrossRef](#)]
13. Zhu, J.; Li, S.; Liao, S.; Xue, Q. Wideband Low-Profile Highly Isolated MIMO Antenna with Artificial Magnetic Conductor. *IEEE Antennas Wirel. Propag. Lett.* **2018**, *17*, 458–462. [[CrossRef](#)]
14. Chatterjee, J.; Mohan, A.; Dixit, V. Broadband Circularly Polarized H-Shaped Patch Antenna Using Reactive Impedance Surface. *IEEE Antennas Wirel. Propag. Lett.* **2018**, *17*, 625–628. [[CrossRef](#)]
15. Huang, J.; Dong, G.; Cai, Q.; Chen, Z.; Li, L.; Liu, G. Dual-Band MIMO Antenna for 5G/WLAN Mobile Terminals. *Micromachines* **2021**, *12*, 489. [[CrossRef](#)]
16. Dou, Y.; Chen, Z.; Bai, J.; Cai, Q.; Liu, G. Two-Port CPW-Fed Dual-Band MIMO Antenna for IEEE 802.11 a/b/g Applications. *Int. J. Antennas Propag.* **2021**, *2021*, 5572887. [[CrossRef](#)]
17. Lu, D.; Wang, L.; Yang, E.; Wang, G. Design of High-Isolation Wideband Dual-Polarized Compact MIMO Antennas with Multiobjective Optimization. *IEEE Trans. Antennas Propag.* **2018**, *66*, 1522–1527. [[CrossRef](#)]
18. Chattha, H.T.; Latif, F.; Tahir, F.A.; Khan, M.U.; Yang, X. Small-Sized UWB MIMO Antenna with Band Rejection Capability. *IEEE Access* **2019**, *7*, 121816–121824. [[CrossRef](#)]